SUPPLEMENTAL FIGURES AND TABLES

A

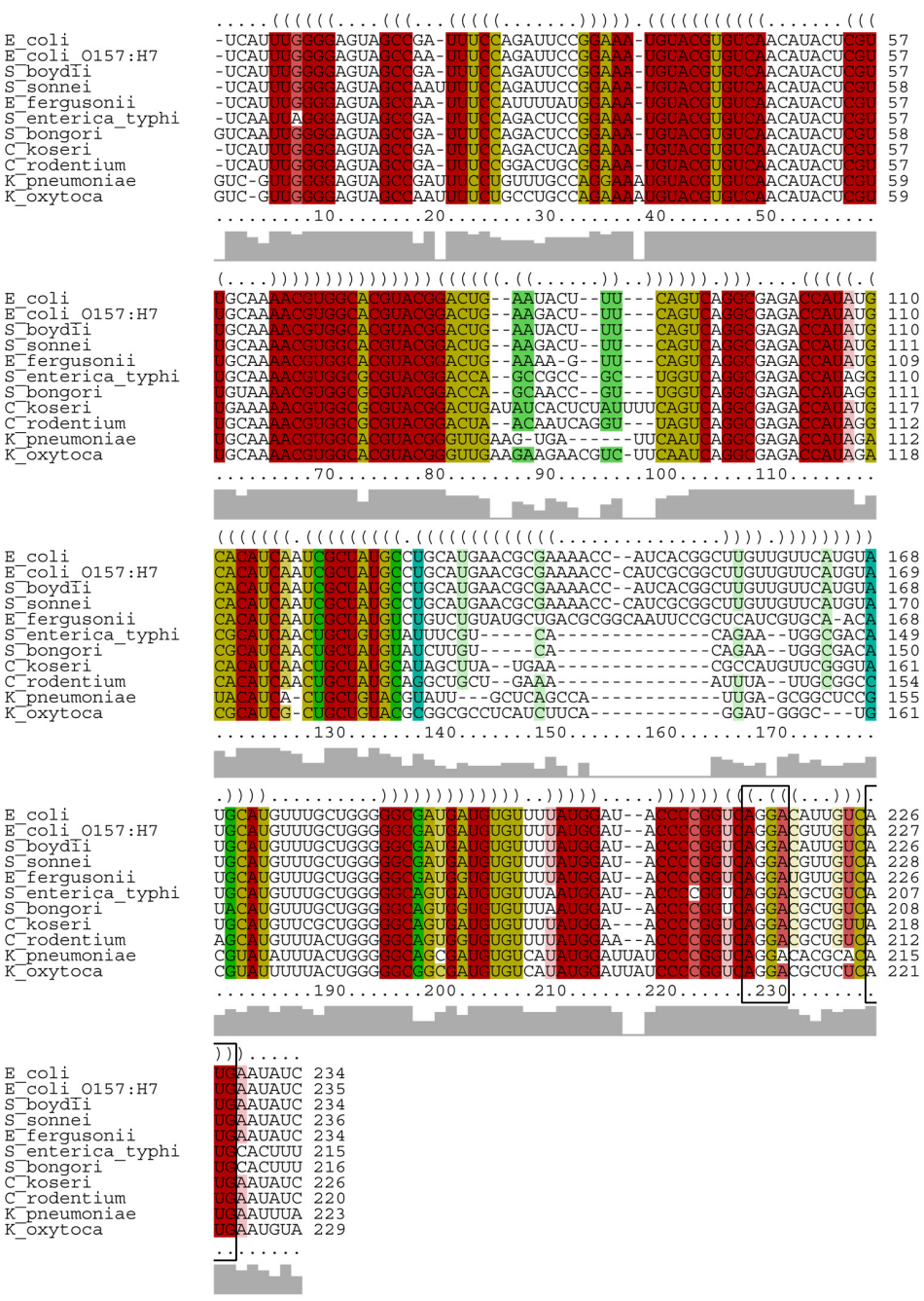

B

construct	-$MnCl_2$	+$MnCl_2$	fold induction
wild type	112 ± 4	459 ± 1	4.1
$A_{108}U_{109}G_{110} \rightarrow U_{108}A_{109}G_{110}$	150 ± 6	514 ± 7	3.4
$A_{191}U_{192}G_{193} \rightarrow U_{191}A_{192}G_{193}$	149 ± 2	526 ± 9	3.8
$A_{226}U_{227}G_{228} \rightarrow U_{226}A_{227}G_{228}$	75 ± 4	80 ± 2	1.1

Figure S1 Conservation of *mntP* secondary structure predicts occlusion of ribosome binding site

(A) Structure-based alignment of the *mntP* riboswitch (5´-UTR) sequences from the +1 through the 3rd codon from *E. coli* and related bacteria was generated using the LocARNA webtool (http://rna.informatik.uni-freiburg.de)(Will et al., 2012). Colors show the number of different possible base-pair combinations at a particular position (red = 1, yellow = 2, green = 3, teal = 4) and extent of conservation (less saturated colors indicate one or more non-base-paired nucleotide at that position). The consensus structure is shown above, parentheses indicate base-paired regions, dots are unpaired nucleotides. Species include *Escherichia coli*, *Escherichia coli O157:H7*, *Shigella boydii*, *Shigella sonnei*, *Escherichia fergusonii*, *Salmonella enterica Typhi*, *Salmonella bongori*, *Citrobacter koseri*, *Citrobacter rodentium*, *Klebsiella pneumoniae* and *Klebsiella oxytoca*. The conserved base pairing potential supports the secondary structure in the predicted "off" conformation of the *mntP* 5´UTR shown in Figure 5A. The ribosome binding site and *mntP* start codon are boxed. Related to Figures 3 and 5.

(B) β-galactosidase activity for strains carrying the indicated mutations in potential alternative start codons in the *mntP* 5´ UTR in the P_{LlacO}-5´UTR_{mntP}-*lacZ* translational fusion. For each construct, residues predicted to base pair with the AUG in the secondary structure in Figure 5A, were mutated to retain base pairing. Cells grown in LB medium were incubated with or without 400 μM $MnCl_2$ for 1 h, and results are given in Miller units as the mean ± SDM of three independent samples. Related to Figure 5.

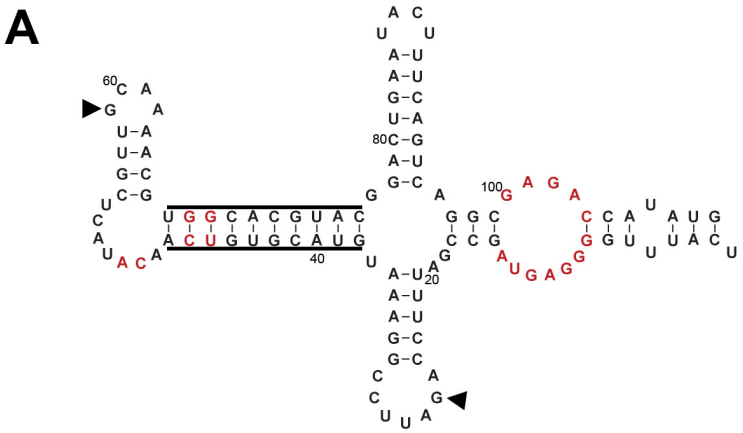
A
60
40
80
100
20

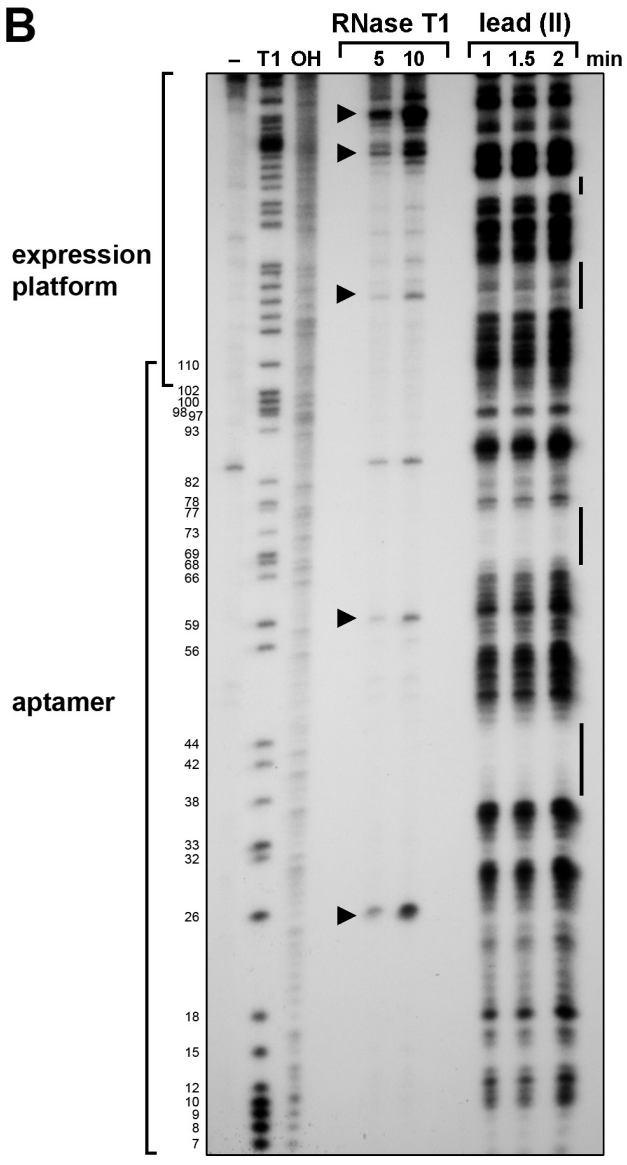
B
RNase T1
lead (II)
– T1 OH
5 10
1 1.5 2 min
expression platform
aptamer
110
102
100
98
97
93
82
78
77
73
69
68
66
59
56
44
42
38
33
32
26
18
15
12
10
9
8
7

Figure S2 Chemical and enzymatic probing of the *mntP* aptamer secondary structure is consistent with sequence conservation and co-variation

(A) Predicted secondary structure of the *mntP* aptamer based on conservation. Nucleotides in red correspond to residues that show >97% sequence conservation in all *yybP-ykoY* representatives identified in genomic databases (Meyer et al., 2011). Related to Figure 3.

(B) Probing of the *mntP* 5′-UTR structure by incubating P^{32}-end labeled, in vitro synthesized RNA with lead and RNase T1, which cleave single stranded nucleotides and 3′ of unpaired G residues, respectively, for the indicated times. Regions with increased RNase T1 cleavage are indicated by arrows. We observe strong cleavage at residues G_{26} and G_{59} in the aptamer domain. These residues are the only predicted G residues located in terminal loops in the proposed secondary structure. Most of the remaining G residues are predicted to comprise portions of helical elements and would thus be impervious to cleavage by RNase T1. However, five G residues present in the conserved central bulge are predicted to be unpaired and thus susceptible to T1 cleavage, but do not produce a band at the corresponding position on our sequencing gel. It is possible that tertiary interactions present in the folded RNA occlude RNase T1 from accessing these G residues. Regions protected from lead cleavage are indicated by the lines. Flexible RNA regions such as unpaired sequences are more susceptible to lead-mediated cleavage than rigid structures such as helical elements (Forconi and Herschlag, 2009). Protected regions observed correspond to residues 38-47 and 67-76, which base pair with each other forming the core of the central helix. We also observe protection from lead mediated cleavage, albeit to a lesser extent, for other regions predicted to base pair. The lesser protection is probably due to the greater conformational entropy resulting from decreased hydrogen bonding potential within these shorter helices. We observe the highest frequency of lead-mediated cleavage in regions that comprise the putative terminal loops predicted in our structure. The band in the RNase T1 lanes above position 82 is present in the untreated control. Related to Figure 3.

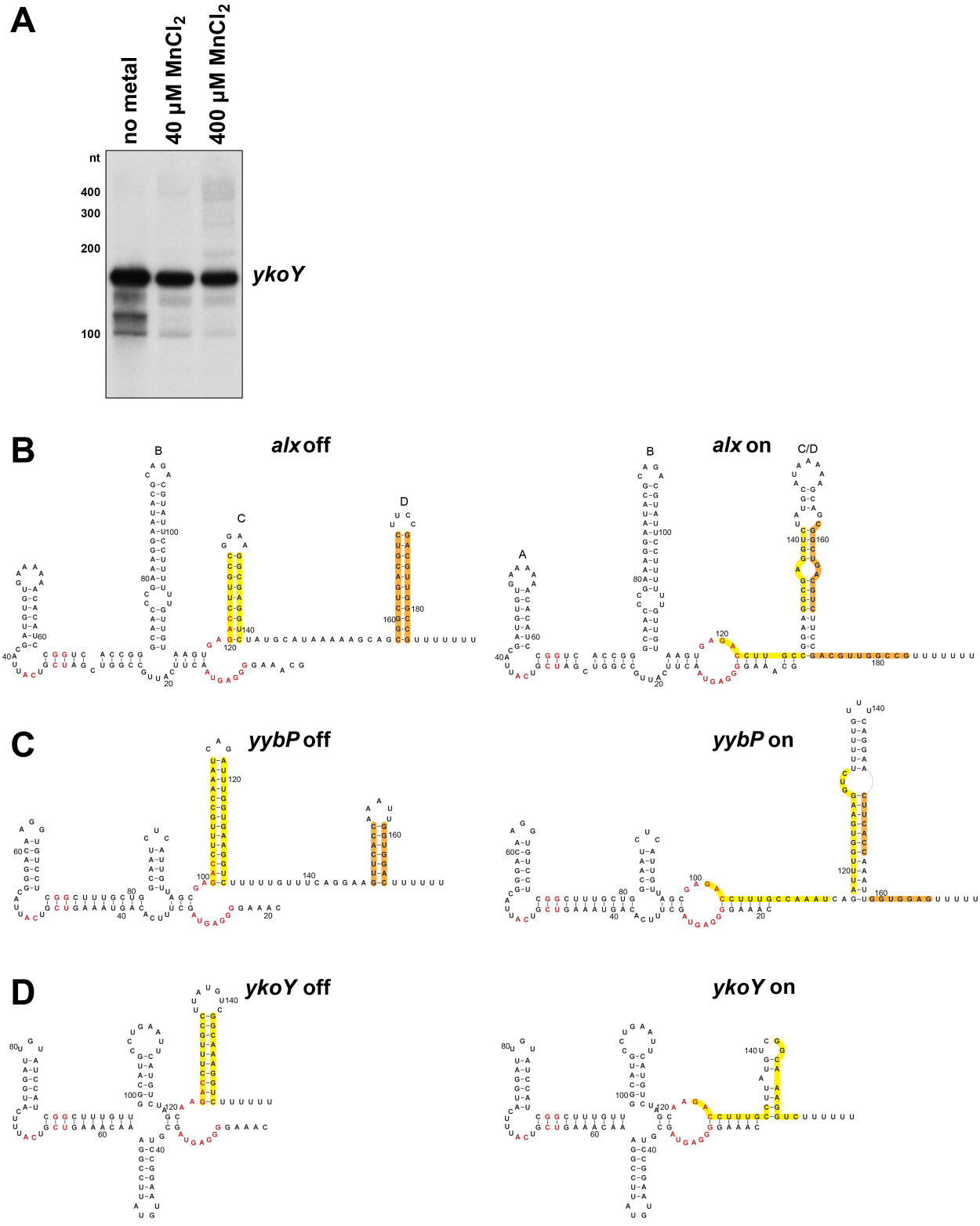
A
no metal
40 µM MnCl2
400 µM MnCl2
nt
400
300
200
100
ykoY
B
alx off
alx on
C/D
C
yybP off
yybP on
D
ykoY off
ykoY on

Figure S3 Predicted secondary structures of *alx*, *yybP* and *ykoY* 5′ UTRs suggest mechanisms of regulation

(A) Longer exposure of Figure 4B.

(B) Predicted structure of the *alx* 5′UTR in the "off" and "on" state. Numbering of nucleotides and labeling of stem-loops is as in (Nechooshtan et al., 2009)

(C) Predicted structure of the *yybP* 5′UTR in the "off" and "on" state.

(D) Predicted structure of the *ykoY* 5′UTR in the "off" and "on" state. Numbering of nucleotides in (C-D) is from the reported 5′ end of the transcripts (Irnov et al., 2010). Predicted structures of the aptamer domains are based on (Barrick et al., 2004). In (B-D), nucleotides in red are conserved in >97% of the *yybP-ykoY* family members (Meyer et al., 2011), while regions predicted to base pair in the absence of Mn^{2+} are highlighted in yellow and orange, respectively.

Upon inspection of the predicted structures of the *alx, yybP*, and *ykoY* 5′-UTRs in the "off" state, we noted a stem-loop structure (highlighted in yellow) immediately after the highly conserved GAGAC motif (red) that comprise the ends of the aptamer in all three riboswitches. By analogy, we predict a similar extended stem-loop structure immediately adjacent to the *mntP* aptamer region (Figure 5A). We also noted that the 5′ end of the RNAs preceding the GGGAGUA motif (red) at the beginning of the aptamer could base-pair with regions of the previously described stem-loop in an alternate conformation. For the *alx, yybP*, and *ykoY* riboswitches, this prevents formation of a transcription terminator in the "on" state. We predict such an interaction in the *mntP* riboswitch similarly would allow an alternate conformation in which the ribosome binding site is released. Related to Figure 5.

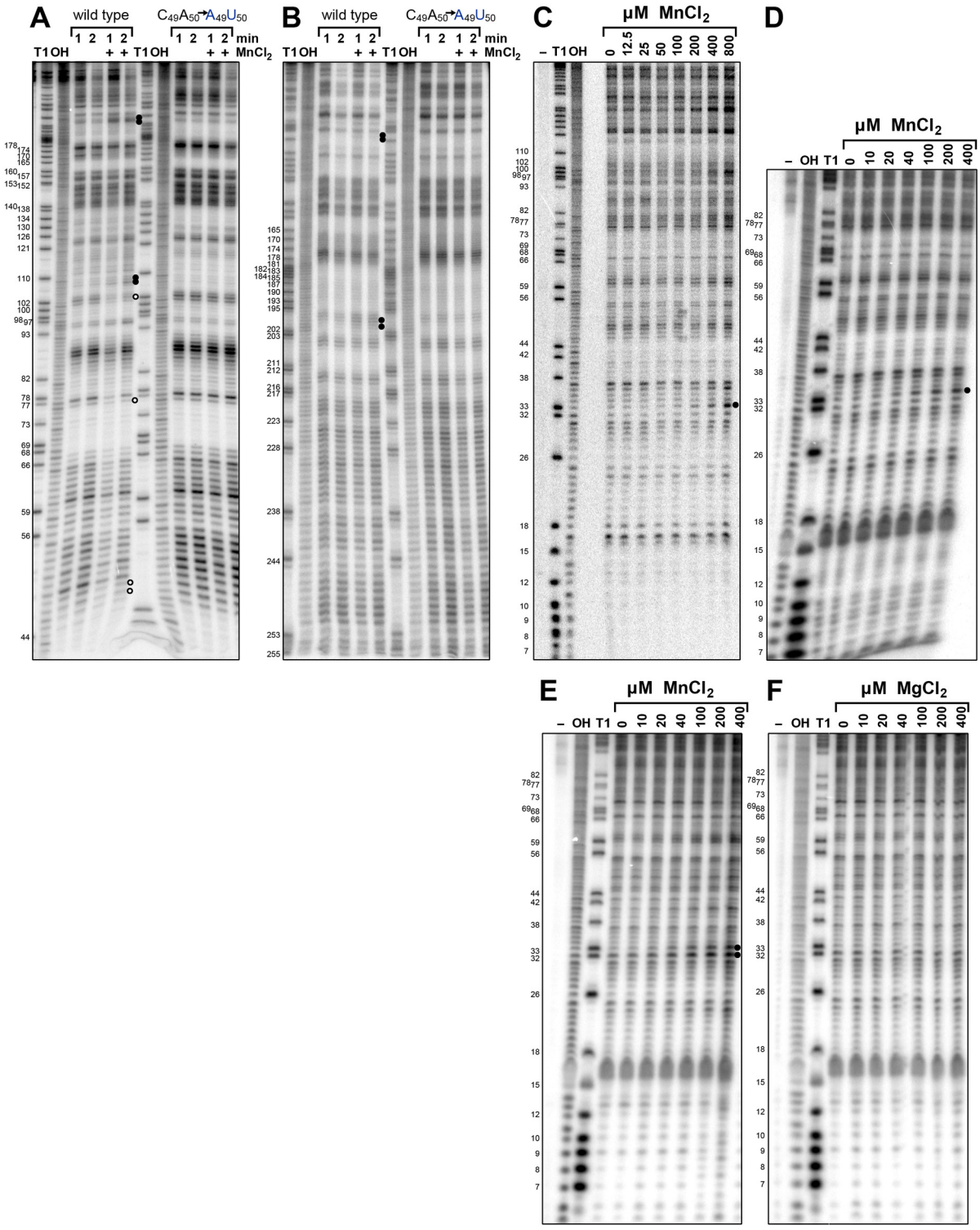
A
wild type
C49A50→A49U50
1 2 1 2
1 2 1 2 min
T1 OH
+ + T1 OH
+ + MnCl2
B
wild type
C49A50→A49U50
1 2 1 2
1 2 1 2 min
T1 OH
+ + T1 OH
+ + MnCl2
C
μM MnCl2
– T1 OH
0 12.5 25 50 100 200 400 800
D
μM MnCl2
– OH T1
0 10 20 40 100 200 400
E
μM MnCl2
– OH T1
0 10 20 40 100 200 400
F
μM MgCl2
– OH T1
0 10 20 40 100 200 400

Figure S4 Lead and inline probing of the *mntP* 5′UTR and aptamer domain reveals limited conformational changes in presence of Mn^{2+}

(A-B) Lead probing of full-length wild type and $C_{49}A_{50}$ mutant *mntP* 5′UTR ^{32}P-end-labeled at the 5′- (A) and 3′- (B) ends incubated with and without $MnCl_2$. Filled circles indicate bands that increase for wild type but not mutant *mntP* in the presence of $MnCl_2$, and open circles indicate those bands that decrease. We consistently observed increased cleavage of nucleotides 107-109 and 197-201.

(C-D) Inline probing of ^{32}P-end-labeled full-length *mntP* 5′UTR (C) and aptamer domain alone (D) in buffer containing 20 mM $MgCl_2$ and the indicated concentrations of $MnCl_2$. A filled circle denotes the band corresponding to the G33 residue that shows increased spontaneous cleavage upon incubation with $MnCl_2$ in both the full-length 5′ UTR and aptamer domain upon incubation for 40 h at room temperature.

(E-F) Inline probing of the *mntP* aptamer domain in buffer containing 2.5 M NaCl substituted for 20 mM $MgCl_2$. Filled circles denote bands corresponding to the G32 and G33 residues showing increased cleavage upon a 40 h, room temperature incubation with $MnCl_2$ (E) but not $MgCl_2$ (F).

Lanes labeled T1 and OH are the nucleotide size markers corresponding to the same labeled *mntP* RNA after cleavage with RNase T1 or hydroxyl anions, respectively. Nucleotide positions from the start of transcription are given to the left of each gel. Related to Figure 5.

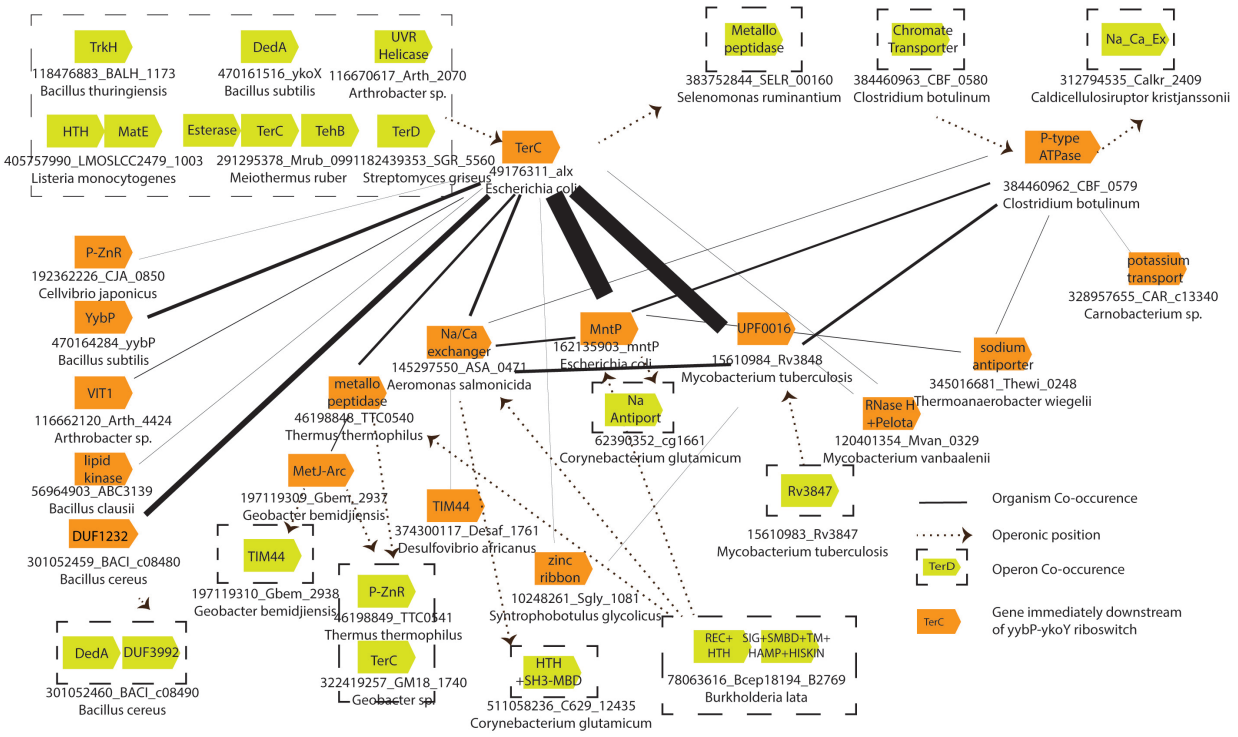

Figure S5 Network of genes immediately downstream of the *yybP-ykoY* riboswitch
The thickness of the edge connecting genes co-occurring in the same genome downstream of a paralogous *yybP-ykoY* motif is scaled as per the frequency of such a co-occurrence in our dataset. The genes that are in the same operon but not immediately downstream of the *yybP-ykoY* riboswitch are shown in boxes with the arrowhead depicting direction of association. The Genbank gi, protein name and organism are shown for representative genes for each node. The domain names are explained in Supplementary Table S2. P-ZnR denotes proteins with a peptidase-associated zinc-ribbon and MetJ-Arc denotes proteins with MetJ-Arc DNA-binding domains. Related to Figure 6.

Nucleic acid	Concentration added to buffer	μM manganese Buffer side	Nucleic acid side	Percent enrichment
wt *mntP* RNA	8	0.8 ± 0.1	9.4 ± 1.0	93%
	40	1.0 ± 0.3	49.4 ± 4.2	98%
	200	0.3 ± 0.04	193.2 ± 7.0	100%
$C_{49}A_{50}$ to $A_{49}U_{50}$ RNA	8	4.3 ± 0.2	6.4 ± 0.5	60%
	40	20.1 ± 1.5	30.7 ± 3.4	60%
	200	85.7 ± 21.7	155.2 ± 15.3	64%
wt *alx* RNA	8	7.3 ± 0.4	4.5 ± 0.8	38%
	40	15.4 ± 0.5	47.8 ± 6.0	75%
	200	70.5 ± 4.7	172.9 ± 0.6	71%
wt *VC1722* RNA	8	4.0 ± 0.2	5.9 ± 0.2	60%
	40	20.0 ± 1.5	28.9 ± 0.6	59%
	200	83.1 ± 2.7	117.9 ± 7.2	59%

Table S1 *mntP* aptamer binding to $MnCl_2$ during equilibrium dialysis
The in vitro synthesized *mntP* aptamer RNA is 109 nucleotides (2 to 110), the *alx* aptamer RNA is 136 nucleotides (1 to 136), and the c-di-GMP aptamer RNA from the *tfoX*-like gene (VC1722) of *Vibrio cholera* is 92 nucleotides (Kulshina et al., 2009). In all cases 100 μM RNA was used in the dialysis. Results are shown for two different experiments. We note that, in most cases, the combined concentration of metal detected by the atomic absorption spectrometer was somewhat higher than the concentration input into the buffer side of the dialysis chamber. This discrepancy may be due to water loss during autoclaving of our $MnCl_2$ stock solutions. The enrichment of $MnCl_2$ in the buffer chamber for the 8 μM *alx* aptamer sample may be due to incomplete equilibration caused by formation of an air bubble at the dialysis membrane. Related to Table 1.

Table S2 Summary of computational analysis of genes downstream of the *yybP-ykoY* motif
Excel tables with computational analysis of genes found downstream of the *yybP-ykoY* motif. "Summary" sheet gives an overview of proteins encoded downstream of the *yybP-ykoY* motif with a description of the domains. "Co-Occurrence" sheet gives matrix showing the frequency of two genes co-occurring in the same genome downstream of a paralogous *yybP-ykoY* motif. "Operon" sheet lists operons for all genes downstream of the *yybP-ykoY* motif identified in complete genomes. "Counts" sheet gives numbers of each type of gene preceded by *yybP-ykoY* motif in each organism. "Organisms" sheet lists all organisms analyzed. Related to Figure 6.

Table S3 Strains and oligonucleotides used in study
Excel tables listing strains and oligonucleotides used in study.

SUPPLEMENTAL EXPERIMENTAL PROCEDURES

Strains and growth conditions. All *E. coli* strains were derived from K-12 MG1655. The *lacZ* fusions were constructed in PM1205 as described previously (Mandin and Gottesman, 2009) with the exception that the P_{BAD} promoter was replaced with the P_{LlacO} promoter in the heterologous promoter fusions. The DNA used for λ-mediated recombination (Court et al., 2003) was generated by PCR using genomic DNA from wild type MG1655 or wild type *lacZ* fusions. The P_{LlacO} containing fusions all begin with the +1 of the 5′-UTR of *mntP* (225 nt upstream of the MntP start codon) or *alx* (206 nt upstream of the Alx start codon) (Thomason et al., 2014) and end with the 15th amino acid of MntP and the 10th amino acid of Alx. All fusions were confirmed by sequencing. Deletions generated by λ-mediated recombination in NM400 or PM1205 or obtained from other laboratories (Battesti et al., 2012) were moved into the desired *lacZ* fusion backgrounds by P1 transduction. All mutations were confirmed by sequencing.

All strains were grown by shaking at 37˚C in either Luria-Bertani (LB) medium (1% bacto-tryptone, 0.5% yeast extract, and 1% NaCl) or minimal M9 medium (Difco) supplemented with 0.2% glucose. Cell density was determined by measuring OD_{600} using an Ultrospec 3300 UV/Vis spectrophotometer (Amersham Biosciences).

In vitro transcription-translation assays. Each RNA was generated using the MEGAscript T7 in vitro transcription system (Ambion) per the manufacturer's instructions. Briefly, each reaction contained 6.4 µg of wild type or mutant PCR template harboring a T7-promoter followed by the entire *mntP* 5′-UTR and ORF with a C-terminal SPA tag. The reactions were incubated at 37˚C for 4 h followed by treatment with 8 units of Turbo DNase (Ambion) for 30 min at 37˚C. Each reaction was subsequently passed through a G-50 microspin column (GE Healthcare) to remove free nucleotides, followed by phenol/chloroform extraction and ethanol precipitation. An aliquot (1 µg) of each RNA was subsequently placed in the PURExpress in vitro protein synthesis kit (New England Biolabs) according to the manufacturers specifications in the presence or absence of 400 µM $MnCl_2$ for 2 h at 37˚C. Aliquots (1.25µl) of the samples were then resolved on a 5-15% SDS-PAGE gel (BioRad) for 1.5 h at 100 V, followed by semi-dry electroblotting onto a nitrocellulose membrane at 25 V and 1.3 Amp for 7 min (PierceG2 Fast Blotter). The membrane was subsequently probed with anti-FLAG M2 monoclonal antibody (Sigma) conjugated to horseradish peroxidase (1:1000) overnight at 4˚C followed by 6 x 5 min washes in TBST (Corning) with 0.1% Tween-20, developed using SuperSignal West Pico Chemiluminescent Substrate (Thermo Scientific) and exposed to X-ray film. Following the transfer, the SDS-PAGE gel was stained using the ProteoSilver-Plus kit (Sigma). RNA was isolated from 5 µl of each sample and analyzed by primer extension as described (Beisel et al., 2012).

RNA isolation and northern analysis. Cultures of the *Bacillus subtilis* strain PY79 grown overnight (~16 h) in LB at 37˚C were incubated for 1 h without or with 40 or 400 µM $MnCl_2$. Cells were collected by centrifugation and flash frozen in liquid nitrogen. Subsequently, cell pellets were rapidly thawed at 37˚C, resuspended in 100 µl of 10 mM TE, pH 8.0 containing 30 mg/ ml lysozyme and placed at 37˚C for 10 min. After two more cycles of flash freezing in liquid nitrogen and thawing at 37˚C, 1 ml of Trizol reagent (Ambion) was added to each sample, and cells were further lysed by repetitive pipetting and then incubated at room temperature for 5 min. After the addition of 0.2 ml of chloroform and further mixing, the top 0.6 ml of the aqueous

phase was transferred to a new tube, extracted once more with Trizol-chloroform. The RNA was precipitated with 0.5 ml of isopropyl alcohol and washed with 75% ethanol before resuspension in 25 µl of deionized water.

For Northern blot analysis, 20 µg of total RNA was separated on an 8% denaturing urea-PAGE gel at 300 V for 1.5 h. The RNA was then transferred to Zeta-probe nylon membranes (BioRad) by electroblotting for 18 h at 20 V at 4˚C. Membranes were UV cross-linked and then incubated in hybridization buffer for 5 h at 45˚C prior to the addition of a P^{32}-labeled oligonucleotide probe. Blots were incubated overnight and then washed 5X in SSC buffer (Corning) and exposed to X-ray film.

Toeprinting assay. Ribosomal 30S subunits were isolated from *E. coli* strain MG1655 via fractionation on sucrose gradients followed by dialysis against 1X extension buffer (10 mM Tris-HCl pH 7.5, 10 mM $MgCl_2$, 60 mM NH_4Cl, 30 mM β-mercaptoethanol). *mntP* RNA was transcribed in vitro using the MEGAscript kit (Ambion) and PCR amplicons consisting of 5´ T7 promoter, the entire *mntP* 5´-UTR and 100 nt of the *mntP* coding sequence. An oligonucleotide complementary to *mntP* (10 nM of 5' P^{32} end labeled MS095) was annealed with 10 nM of the in vitro synthesized RNA by dilution in 1X extension buffer, heating to 65˚C for 5 min and slow cooling to 37˚C for 30 min. Toeprinting assays were performed by adding 60 nM 30S ribosomes, 120 nM $fMet^{tRNA}$ (Sigma Aldrich), 375 µM dNTPs, and 400 µM $MnCl_2$ to a final volume of 19 µl in 1X extension buffer, after which 1 µl (1 U) of reverse transcriptase (AMV) was added to each reaction. The reactions were incubated at 37˚C for 15 min and then stopped by the addition of 20 µl gel loading dye. Reactions were separated by PAGE (8% polyacrylamide, 7 M urea) and visualized by exposure to X-ray film. A sequencing ladder was generated using the same radiolabeled oligonucleotide, the above *mntP* PCR amplicon and SequiTherm Excel II kit (Epicentric Biotechnologies).

RNA radiolabeling and in vitro structure probing. For T7 transcription using the MegaShortscript T7 Transcription Kit (Ambion), about 24 pmol of RNA was dephosphorylated and then labeled with ^{32}P at the 5´ end with T4 polynucleotide kinase (New England Biolabs) or 3´ end with single stranded RNA ligase (New England Biolabs) per the manufacturer's instructions. Following gel purification, the radiolabeled RNA was extracted with RNA elution buffer (0.1 M NaO_2CCH_3, 0.1% SDS, 10 mM EDTA) overnight at 4˚C. The eluate was phenol-choroform extracted and ethanol precipitated. RNase T1 cleavage was carried out in 10X RNA Structure buffer (Ambion). Lead cleavage was carried out as described previously (Beisel et al., 2012). In-line probing was performed as described previously (Wakeman and Winkler, 2009). End-labeled *mntP* RNA (~5 pmol) was mixed with 2X in-line buffer (100 mM Tris-HCl pH 8.3, 200 mM NaCl, 20 mM $MgCl_2$) or modified 2X in-line buffer (100 mM Tris-HCl pH 8.3, 5 M NaCl), and a range of $MnCl_2$ concentrations in a final volume of 10 µl and incubated 39-48 h at room temperature. All RNA samples were resolved by electrophoresis on 8% polyacrylamide/7M Urea gels. Size markers were generated by incubating denatured ^{32}P-radiolabeled *mntP* RNA in 1X Alkaline Hydrolysis buffer (Ambion) or with RNase T1 in 1X RNA Sequencing buffer (Ambion).

Computational analysis of the *yybP-ykoY* motif. The covariance model for the motif was prepared using the complete alignment of the *yybP-ykoY* riboswitch provided by the Rfam database (Burge et al., 2013). The model was searched against the prokaryotic reference set of

genomes of 2755 organisms using the CMSEARCH program of the Infernal 1.1 package (Nawrocki and Eddy, 2013). The program uses a filter pipeline for RNA homology search based on accelerated profile hidden Markov model (HMM) methods and HMM-banded CM alignment methods, which, in benchmarks with a reference set of riboswitches (Barrick et al., 2004), out-performed other CM-based as well as BLASTN based detection methods. The threshold for inclusion in our collection was an e-value of .01 and all alignments with e>.005 were examined visually to exclude false positives. The detected riboswitches were then loaded onto gene neighborhoods extracted from the GenBank files from the genomes using in-house Perl scripts and operons were predicted using co-directionality and intergenic distance constraints. The encoded proteins were analyzed using the iterative sequence-profile using PSI-BLAST (Schäffer et al., 2001), and HMM searches were performed using JackHMMER (Johnson et al., 2010). Profile-profile comparisons were performed using the HHpred program (Hildebrand et al., 2009).

SUPPLEMENTAL REFERENCES

Barrick, J.E., Corbino, K.A., Winkler, W.C., Nahvi, A., Mandal, M., Collins, J., Lee, M., Roth, A., Sudarsan, N., Jona, I.*, et al.* (2004). New RNA motifs suggest an expanded scope for riboswitches in bacterial genetic control. Proc Natl Acad Sci USA *101*, 6421-6426.

Battesti, A., Tsegaye, Y.M., Packer, D.G., Majdalani, N., and Gottesman, S. (2012). H-NS regulation of IraD and IraM antiadaptors for control of RpoS degradation. J Bacteriol *194*, 2470-2478.

Beisel, C.L., Updegrove, T.B., Janson, B.J., and Storz, G. (2012). Multiple factors dictate target selection by Hfq-binding small RNAs. EMBO J *31*, 1961-1974.

Burge, S.W., Daub, J., Eberhardt, R., Tate, J., Barquist, L., Nawrocki, E.P., Eddy, S.R., Gardner, P.P., and Bateman, A. (2013). Rfam 11.0: 10 years of RNA families. Nucleic Acids Res *41*, D226-D232.

Court, D.L., Swaminathan, S., Yu, D., Wilson, H., Baker, T., Bubunenko, M., Sawitzke, J., and Sharan, S.K. (2003). Mini-λ: a tractable system for chromosome and BAC engineering. Gene *315*, 63-69.

Forconi, M., and Herschlag, D. (2009). Metal ion-based RNA cleavage as a structural probe. Methods Enzymol *468*, 91-106.

Hildebrand, A., Remmert, M., Biegert, A., and Söding, J. (2009). Fast and accurate automatic structure prediction with HHpred. Proteins *77*, 128-132.

Irnov, I., Sharma, C.M., Vogel, J., and Winkler, W.C. (2010). Identification of regulatory RNAs in *Bacillus subtilis*. Nucleic Acids Res *38*, 6637-6651.

Johnson, L.S., Eddy, S.R., and Portugaly, E. (2010). Hidden Markov model speed heuristic and iterative HMM search procedure. BMC Bioinformatics *11*, 431.

Kulshina, N., Baird, N.J., and Ferré-D'Amaré, A.R. (2009). Recognition of the bacterial second messenger cyclic diguanylate by its cognate riboswitch. Nat Struct Mol Biol *16*, 1212-1217.

Mandin, P., and Gottesman, S. (2009). A genetic approach for finding small RNAs regulators of genes of interest identifies RybC as regulating the DpiA/DpiB two-component system. Mol Microbiol *72*, 551-565.

Meyer, M.M., Hammond, M.C., Salinas, Y., Roth, A., Sudarsan, N., and Breaker, R.R. (2011). Challenges of ligand identification for riboswitch candidates. RNA Biol *8*, 5-10.

Nawrocki, E.P., and Eddy, S.R. (2013). Infernal 1.1: 100-fold faster RNA homology searches. Bioinformatics *29*, 2933-2935.

Nechooshtan, G., Elgrably-Weiss, M., Sheaffer, A., Westhof, E., and Altuvia, S. (2009). A pH-responsive riboregulator. Genes Dev *23*, 2650-2662.

Schäffer, A.A., Aravind, L., Madden, T.L., Shavirin, S., Spouge, J.L., Wolf, Y.I., Koonin, E.V., and Altschul, S.F. (2001). Improving the accuracy of PSI-BLAST protein database searches with composition-based statistics and other refinements. Nucleic Acids Res *29*, 2994-3005.

Thomason, M.K., Bischler, T., Eisenbart, S.K., Förstner, K.U., Zhang, A., Herbig, A., Nieselt, K., Sharma, C.M., and Storz, G. (2014). Global transcriptional start site mapping using dRNA-seq reveals novel antisense RNAs in *Escherichia coli*. J Bacteriol *197*, 18-28.

Wakeman, C.A., and Winkler, W.C. (2009). Structural probing techniques on natural aptamers. Methods Mol Biol *535*, 115-133.

Will, S., Joshi, T., Hofacker, I.L., Stadler, P.F., and Backofen, R. (2012). LocARNA-P: Accurate boundary prediction and improved detection of structural RNAs. RNA *18*, 900-914.